Dynamic Nuclear Spin Resonance in *n*-GaAs

Y. S. Chen,[1,*] D. Reuter,[2] A. D. Wieck,[2] and G. Bacher[1]

[1]*Werkstoffe der Elektrotechnik and CeNIDE, Universität Duisburg-Essen, Bismarckstraße 81, D-47057 Duisburg, Germany*
[2]*Lehrstuhl für Angewandte Festkörperphysik, Ruhr-Universität Bochum, Universitätsstraße 50, D-44780 Bochum, Germany*

(Received 8 June 2011; published 12 October 2011)

The dynamics of optically detected nuclear magnetic resonance is studied in *n*-GaAs via time-resolved Kerr rotation using an on-chip microcoil for rf field generation. Both optically allowed and optically forbidden NMR are observed with a dynamics controlled by the interplay between dynamic nuclear polarization via hyperfine interaction with optically generated spin-polarized electrons and nuclear spin depolarization due to magnetic resonance absorption. Comparing the characteristic nuclear spin relaxation rate obtained in experiment with master equation simulations, the underlying nuclear spin depolarization mechanism for each resonance is extracted.

DOI: 10.1103/PhysRevLett.107.167601 PACS numbers: 76.70.Hb, 76.60.Es, 76.70.Fz, 78.47.db

Nuclear magnetic resonance represents a technique widely utilized to address nuclei in various materials, e.g., in order to analyze the local nuclear spin environment [1]. Recent progress in quantum information processing requires an in depth understanding of nuclear spins [2,3] particularly in semiconductor quantum structures, where the nuclear properties are varying on a mesoscopic length scale [4–7]. The ability of dynamic nuclear spin polarization via hyperfine interaction with spin-polarized electrons greatly facilitates access to the nuclear spins in semiconductors via NMR experiments [8,9]. These results give insight, e.g., into the dipole-dipole (DD) interaction strength [10,11] or the impact of the nuclear quadrupole (NQ) interaction under a local electrical field from atomic distortion [8,12], doping (defects) [13],or strain [14]. Such local perturbations can cause a mixing of nuclear spin states and thus induce optically forbidden, nonfundamental magnetic resonances by rf absorption. Usually, the properties of the nuclear spins are extracted from either spectral features of the NMR signal, like spectral broadening and spectral shift, or spin-echo types of experiments. Qualitatively new insights into the nuclear spin dynamics in semiconductors are expected by investigating the transient nuclear spin properties, in particular, under nonfundamental resonance conditions. This, however, has not been reported for any semiconductor to our knowledge.

Here, we present optically detected NMR experiments, where optically generated spin-polarized electrons align the nuclear spins via dynamic nuclear polarization (DNP). An on-chip microcoil is used to temporally switch the rf excitation selectively for fundamental as well as nonfundamental NMR. The dynamical change of the nuclear spin polarization is probed by time-resolved Kerr rotation (TRKR) measurements. Interestingly, a very specific nuclear spin dynamics is found for each kind of resonance (fundamental, second-harmonics, mixed resonances, and half-harmonics). Comparing the experimental data with numerical calculations allows for each resonance a direct identification of the predominant nuclear spin depolarization path.

The measurements were performed on a Si-doped GaAs sample, grown with molecular beam epitaxy on a GaAs (100) substrate. The active region has a doping concentration of 5×10^{16} cm^{-3} and a thickness of 2 μm. It is sandwiched between an undoped GaAs layer of 50 nm thickness below and a Si-doped GaAs layer above. The latter one is gradually doped up to an electron density of 5×10^{18} cm^{-3} within 15 nm and followed by another 15 nm thick GaAs layer with a constant doping level of 5×10^{18} cm^{-3}. This avoids band bending effects within the active layer due to surface depletion. In an oblique geometry with an incident angle of $\theta_1 \approx 18°$ (see inset of Fig. 1), circularly polarized optical pumping is utilized to generate spin-polarized electrons, and the contact

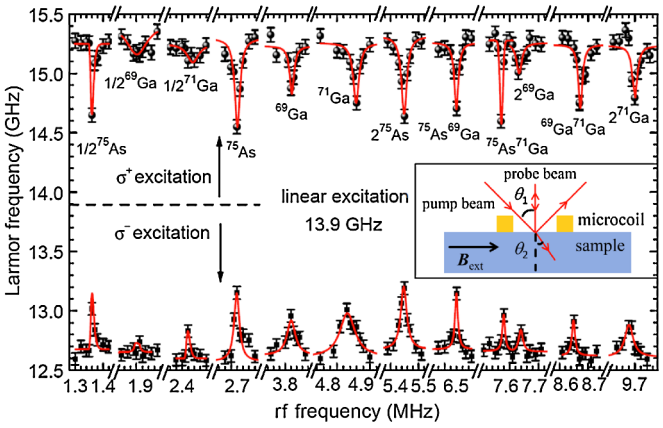

FIG. 1 (color online). Optically detected NMR under σ^+—polarized optical excitation (balls) and σ^-—polarized optical excitation (squares). The horizontal dashed line indicates the Larmor frequency measured under linear polarized excitation. Lines are a guide to the eyes. The inset schematically shows the geometry of the experiment. $\theta_1 \sim 18°$ for the pump beam and $\theta_1 \sim 0°$ for the probe beam is used in the experiment.

hyperfine interaction gives rises to a nuclear spin polarization [8]. As a result of the DNP formation, the electrons experience an additional nuclear field $\boldsymbol{B}_N$ (namely the Overhauser field) along with the static external in-plane field $\boldsymbol{B}_{\text{ext}}$ of 374 mT. The nuclear spin dynamics is traced by monitoring the electron Larmor precession frequency $\boldsymbol{\omega}_L(t) = g^*\mu_B[\boldsymbol{B}_{\text{ext}} + \boldsymbol{B}_N(t)]/\hbar$, where g^* is the electron Landé g factor, via a linearly polarized probe beam. The local rf field is provided by an on-chip Au microcoil with an inner diameter of about 19 μm, which is realized atop the semiconductor by electron beam lithography and lift-off technique [15,16].

We use TRKR measurements to track the electron Larmor precession frequency ω_L [16] for gaining insight into the nuclear spin dynamics under rf excitation. For linear optical excitation the characteristic electron Larmor frequency is found to be ~13.9 GHz (see dashed line in Fig. 1). Using right circularly polarized (σ^+) excitation until DNP saturation, ω_L changes to ~15.2 GHz indicating an Overhauser field $\boldsymbol{B}_N$ parallel to $\boldsymbol{B}_{\text{ext}}$. In the case of left circularly polarized (σ^-) excitation, $\boldsymbol{B}_N$ is antiparallel to $\boldsymbol{B}_{\text{ext}}$ resulting in a reduction of ω_L down to ~12.6 GHz. From the data, we estimate a saturation Overhauser field of about 35 mT (corresponding to a nuclear spin polarization of ~0.66% [17]) for our experimental conditions [18].

To perform NMR experiments, a switchable rf field with a magnitude of ~1.2 mT is generated from the on-chip microscale current loop [16]. For the NMR experiments discussed in the following, optical excitation is always on and DNP gets saturated prior to the rf excitation being switched on. In a first experiment, the radio frequency is varied and for each frequency, a complete TRKR curve is recorded for getting a very precise value of the Larmor frequency. Nuclear spin depolarization is observed at different resonance frequencies and the Larmor frequency ω_L is clearly reduced (enhanced) for σ^+ (σ^-) optical excitation. The observed NMR results are presented in Fig. 1. They can be classified as four types: (1) fundamental NMR at frequencies of $f^\alpha = \gamma^\alpha B_{\text{ext}}$ [7–11,13,14,16,17,19], where γ^α is the nuclear gyromagnetic ratio of isotope species α; (2) two-spin NMR involving one isotope species at $2f^\alpha$ [10,13,19]; (3) two-spin NMR involving different species of isotopes at $(f^{\alpha 1} + f^{\alpha 2})$ [19]; (4) half-harmonic NMR at $1/2f^\alpha$ [12,19,20].

In order to understand the occurrence of the nonfundamental NMR, the nuclear spin Hamiltonian is written as:

$$\boldsymbol{H} = \boldsymbol{H}_Z + \boldsymbol{H}_{\text{hf}} + \boldsymbol{H}_{\text{rf}} + \boldsymbol{H}_{\text{DD}} + \boldsymbol{H}_{\text{NQ}}. \quad (1)$$

The first two terms refer to the Zeeman energy and the hyperfine interaction, respectively. $\boldsymbol{H}_{\text{rf}}$ is the perturbation arising from the rf magnetic field, $\boldsymbol{H}_{\text{DD}}$ is related to the dipole-dipole interaction, and $\boldsymbol{H}_{\text{NQ}}$ represents the nuclear quadrupole interaction. By using Ladder operators [1], we could see that $\boldsymbol{H}_{\text{rf}}$, $\boldsymbol{H}_{\text{DD}}$, and $\boldsymbol{H}_{\text{NQ}}$ contribute to the off-diagonal elements in (1). The latter two cause a mixture of nuclear spin states with $\Delta I = 1$, where I is the nuclear spin component along the $\boldsymbol{B}_{\text{ext}}$ direction. As a consequence, optically forbidden spin transitions with $\Delta I = 2$ become possible under magnetic resonance conditions [8,10,19]. For the DD interaction, spin coupling can be between neighboring nuclei of either the same isotope species or between two different kinds of isotopes, which allows $\boldsymbol{H}_{\text{DD}}$ to induce NMR at $2f^\alpha$ and at $(f^{\alpha 1} + f^{\alpha 2})$, respectively. Since nuclear quadrupole interaction only involves one nucleus (for each isotope species in GaAs the quadrupole moment is nonzero), $\boldsymbol{H}_{\text{NQ}}$ can consequently induce the $2f^\alpha$ resonance.

The half-harmonic resonance at $1/2f^\alpha$ suggests two-quanta rf absorption for spin transitions of $\Delta I = 1$, which stems from the oscillating rf field oblique to the nuclear field [21]. This geometry can happen in case of either strong nuclear quadrupole interaction with the crystal field if the applied rf field is perpendicular to $\boldsymbol{B}_{\text{ext}}$ [8,12], or the applied rf field is intentionally oblique to $\boldsymbol{B}_{\text{ext}}$ [20]. As the quadrupole field around donors is on the order of 0.1 mT [16,22], which is quite small compared with $B_{\text{ext}} = 374$ mT, this hardly changes the parallelism of $\boldsymbol{B}_N$ and $\boldsymbol{B}_{\text{ext}}$. However, the transverse field component $\boldsymbol{B}_{\text{rf-tran}}$ (parallel to $\boldsymbol{B}_{\text{ext}}$) varies within the microcoil center and can achieve values on the order of 1 mT in the metal vicinity, thus resulting in $\boldsymbol{B}_N$, which is oblique to the total rf field. We attribute this spatially inhomogeneous rf field from the on-chip microcoil to be responsible for the $1/2f^\alpha$ NMR.

In the second set of experiments, we make use of the fact that the rf field provided by the microcoil can be switched on a sub-ns time scale [23], which allows us to trace the nuclear spin dynamics under resonance conditions. Two typical TRKR data sets obtained under rf resonance conditions are presented in Fig. 2(a). The arrows mark the time when the rf field was switched on. In the case of the fundamental ^{75}As NMR (upper panel), there is an abrupt change of the Kerr rotation signal after switching on the rf field, while for the ^{75}Ga^{75}As resonance (lower panel), the TRKR signal changes on a time scale of minutes. The variation of the Larmor frequency $\boldsymbol{\omega}_L$ with lab time after switching on the rf field is plotted for a few selected resonances in Fig. 2(b). Each curve could be roughly fitted by a monoexponential decay with a nuclear spin relaxation (NSR) time constant $\tau_{\text{NSR}}(\text{exp})$ as summarized in Table I. For the fundamental resonances, $\tau_{\text{NSR}}(\text{exp})$ is much shorter than 1 min and limited by our experiment, i.e., the time needed for recording one TRKR curve. In the case of the $2f^\alpha$ and the $1/2f^\alpha$ resonances, $\tau_{\text{NSR}}(\text{exp})$ is on the order of 1 min, while for the $(f^{\alpha 1} + f^{\alpha 2})$ resonances, time constants between 2.4 and 4.2 min are extracted from the data.

It has to be noted that the nuclei are always exposed to polarized optical excitation and thus experience DNP formation during the measurements. Thus, the nuclear spin

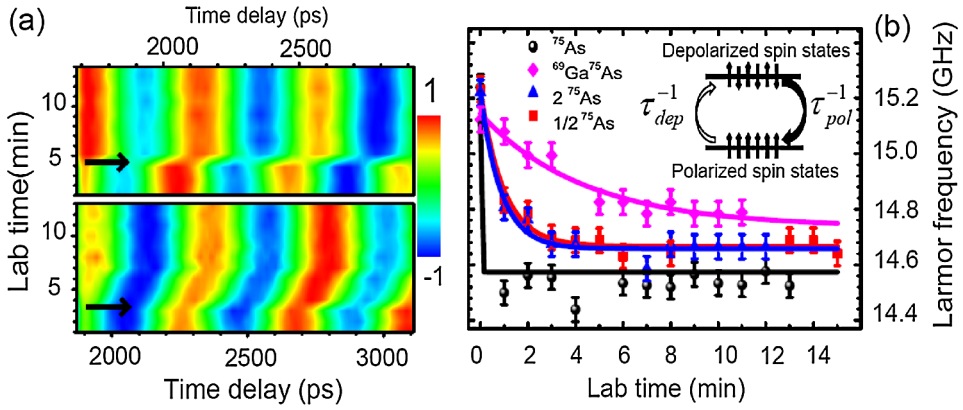

FIG. 2 (color online). (a) 2D plot of the Kerr rotation data. The color code describes the amplitude of the Kerr signal and the arrows indicate the lab time, where the rf field is switched on. The data for the upper plot are obtained at the ^{75}As NMR, while the lower plot represents the data recorded for the ^{71}Ga^{75}As NMR. (b) Larmor frequency versus lab time for different resonances (symbols). The solid lines are monoexponential fits. Inset: Two-level scheme used for describing the nuclear spin dynamics.

dynamics can be described by a two-level model as shown in the inset of Fig. 2(b). The nuclear spin polarization with a rate $\tau_{\mathrm{pol}}{}^{-1}$ caused by the hyperfine interaction $\boldsymbol{H}_{\mathrm{hf}}$ competes with the depolarization due to rf absorption with a rate $\tau_{\mathrm{dep}}{}^{-1}$. By solving the rate equation for the dynamic Overhauser field $dB_N/dt = (B_{N0} - B_N)/\tau_{\mathrm{pol}} - B_N/\tau_{\mathrm{dep}}$, the nuclear spin relaxation rate and the reduction of the Overhauser field ΔB_N at resonance conditions are obtained as $\tau_{\mathrm{NS}}{}^{-1} = (\tau_{\mathrm{pol}}{}^{-1} + \tau_{\mathrm{dep}}{}^{-1})$ and $\Delta B_N = B_{N0}/(1 + \tau_{\mathrm{dep}}/\tau_{\mathrm{pol}})$, respectively. Here, B_{N0} is the Overhauser field in case of DNP saturation.

In order to determine the polarization time τ_{pol}, TRKR measurements with defined rf switching sequences were performed as shown in Fig. 3(a). By using σ^+—polarized optical pumping without an applied rf field, the DNP formation results in an increase of the Overhauser field with a characteristic time constant of $\tau_{\mathrm{pol,exp}} = 9.4$ min. After saturation, the rf field is switched on with a frequency resonant to the ^{75}As isotope and the ^{75}As nuclear spins are depolarized instantaneously, i.e., below the time scale of our experiment. Afterwards, the rf field is again switched off and the ^{75}As nuclei get polarized with a time constant of 4.6 min. This difference in the time constants is related to the fact that the first DNP process involves all three species of isotopes, while the latter one is only controlled by the DNP of the ^{75}As nuclei.

According to Ref. [24], one obtains for the DNP formation time for the isotope species α the relation $\tau_{\mathrm{pol}-\alpha} \sim f_{l-\alpha} \cdot \chi_\alpha(\gamma_\alpha P_{f-\alpha})^{-2}$, where $f_{l-\alpha}$ is the nuclear spin leakage factor, χ_α is the isotope abundance, and $P_{f-\alpha}$ is electron probability density at the nucleus normalized by the unit cell volume [1,24]. By comparing the experimental nuclear field amplitude with the theoretically expected one for each isotope species [16,17], the leakage factor relation is obtained as $f_{l-^{75}\mathrm{As}}{:}f_{l-^{69}\mathrm{Ga}}{:}f_{l-^{71}\mathrm{Ga}} \approx 20{:}16{:}25$. Using the assumption $\tau_{\mathrm{pol}} = \Sigma\tau_{\mathrm{pol}-\alpha}$, the value $\tau_{\mathrm{pol}-\alpha}$ for each isotope species α can be estimated. From $\tau_{\mathrm{pol,exp}} = 9.4$ min, $\tau_{\mathrm{pol}-^{75}\mathrm{As}} = 5.0$ min is extracted, which fairly well agrees with the experimental value of 4.6 min. Similar experiments have been performed for the ^{71}Ga isotope, where $\tau_{\mathrm{pol}-^{71}\mathrm{Ga}} = 2.77$ min is measured, in good agreement with the calculated value of 2.8 min. In Table I, the extracted polarization time for each NMR is listed. Hereby, we assume $\tau_{\mathrm{pol}} = (\tau_{\mathrm{pol}-\alpha 1} + \tau_{\mathrm{pol}-\alpha 2})$ for the $(f^{\alpha 1} + f^{\alpha 2})$ resonances [25].

In order to determine the depolarization time τ_{dep} we consider the different depolarization mechanisms for each NMR. The temporal evolution of nuclear spin states can be described by the Lindblad master equation [26]:

$$\frac{d\rho}{dt} = \frac{1}{i\hbar}[H, \rho] + (2L\rho L^\dagger - \{L^\dagger L, \rho\}), \qquad (2)$$

TABLE I. Experimentally obtained time constant of the nuclear spin relaxation $\tau_{\mathrm{NSR}}(\mathrm{exp})$, based on the average values measured for σ^+—and σ^-—excitation (second column). In the third column, the nuclear polarization time τ_{pol} is listed as extracted from the data presented in Fig. 3(a). The last column summarizes the depolarization time constant τ_{dep} as obtained from the numerical simulations. All the presented constants are in a time unit of minutes.

NMR	$\tau_{\mathrm{NSR}}(\mathrm{exp})$	τ_{pol}	$D - D$	τ_{dep} NQ	B_{tran}
^{69}Ga^{75}As	4.2	6.6	6.0	⋯	⋯
^{71}Ga^{75}As	2.7	7.8	5.6	⋯	⋯
^{69}Ga^{71}Ga	2.4	4.4	3.6	⋯	⋯
2 ^{75}As	0.8	5.0	19	0.05 [1.2]	⋯
2 ^{71}Ga	1.0	2.8	7.2	0.03 [0.4]	⋯
1/2^{75}As	1.1	5.0	⋯	⋯	1.3
1/2^{71}Ga	0.9	2.8	⋯	⋯	0.5
^{75}As	$\ll 1$	5.0		$\ll 1$	

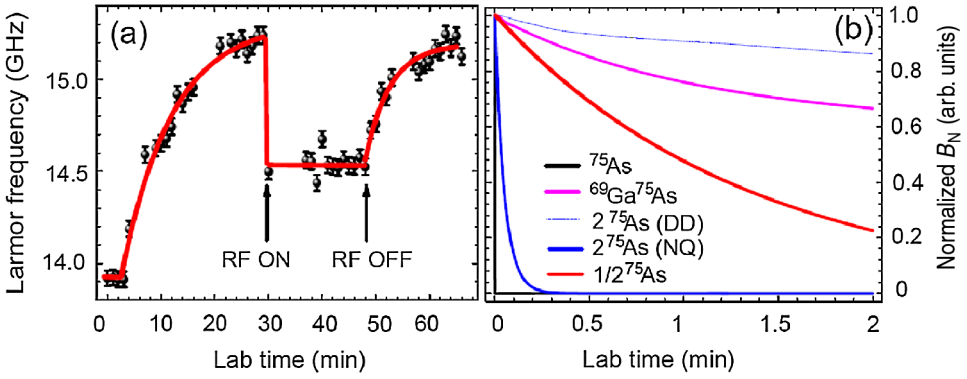

FIG. 3 (color online). (a) Larmor frequency ω_L versus lab time for a well-defined rf switching sequence. Lines are a guide to the eyes. (b) Numerically calculated temporal variation of the nuclear field assuming nuclear spin depolarization purely due to magnetic resonance absorption.

where $\boldsymbol{H} = \boldsymbol{H}_Z + \boldsymbol{H}_{\rm rf} + \boldsymbol{H}_{\rm DD} + \boldsymbol{H}_{\rm NQ}$ is the nuclear spin Hamiltonian, ρ is the nuclear spin density matrix, and L the Lindblad operator. As the nuclear spin relaxation via thermal vibrations is negligible in the low temperature regime used here [24], the Lindblad operator can be simplified as $L = \Gamma\sigma_z$, where Γ is a constant determining the nuclear spin-spin relaxation rate and σ_z is the Pauli matrix.

To simulate the NMR-induced nuclear spin depolarization process, the following steps are performed: (i) the initial nuclear spin polarization degree is set to unity; (ii) in a first approximation, a nuclear spin-spin relaxation time of $T_2 = 100\ \mu$s is taken for all three isotope species using the measured Rabi coherence time $T_2^{\rm Rabi}$ of the ^{75}As isotope (assuming $T_2^{\rm Rabi} \approx 2^* T_2$) [1,16]; (iii) the relaxation rate Γ is defined as the nuclear spin-spin relaxation rate relative to the instantaneous total magnetic field [27]; (iv) for the calculations of the NQ-induced NMR, the quadrupole field magnitude is taken from literature as 0.4 mT for the ^{75}As and 0.3 mT for the ^{71}Ga isotope, respectively [22]. For the calculations of the $1/2f^{\alpha}$ NMR, a transverse field of $B_{\rm rf\text{-}tran} = 0.15$ mT as a calculated averaged value inside the microcoil is used.

Under these assumptions, the nuclear spin depolarization dynamics is numerically calculated from the master equation. Finally, the total dynamic nuclear field experienced by the precessing electrons is determined by weighting the nuclear field amplitude of each isotope with the respective isotope spin polarization. The calculated temporal evolution of the nuclear field is presented in Fig. 3(b). From the numerical calculations, the characteristic decay time constants are extracted and listed in Table I.

There are several interesting features that need to be discussed here. First, nuclear spin depolarization at the fundamental resonance is on the order of 100 μs, determined by the nuclear spin-spin relaxation time. Second, for the nonfundamental NMR, the nuclear spin depolarization occurs on a quite long time scale of minutes, in good agreement with our experimental findings. Hereby, the DD-induced spin depolarization is generally much slower than the spin depolarization caused by the transverse field component $B_{\rm rf\text{-}tran}$ and the NQ interaction, respectively. This is basically due to its much smaller perturbation strength, which is on the order of 0.01 mT or less in GaAs [10]. From the calculated data, the local NQ perturbation is identified as the dominant factor limiting the depolarization of the observed $2f^{\alpha}$ NMR. Note that the NQ field mainly depolarizes the nuclear spins located in the vicinity of the donors. Thus, a finite spin diffusion time $\tau_{\rm diff}$ has to be considered for getting the total depolarization time [28]. The values given in squared brackets in Table I indicate the expected spin diffusion time by taking into account the average distance between neighboring donors in our sample. The DD interaction strength is enhanced for the $(f^{\alpha 1} + f^{\alpha 2})$ resonances due to shorter internucleus distance, generating a faster spin depolarization as compared to the DD-induced depolarization of the $2f^{\alpha}$ NMR. For the $1/2f^{\alpha}$ NMR, the nuclear spin depolarization time is calculated based on the average value of $B_{\rm rf\text{-}tran}$ inside the microcoil.

A quite good agreement between theory and experiment is obtained allowing an identification of the dominant depolarization mechanism for each NMR resonance observed in the experiment. In order to further prove the validity of our results, the change of the Larmor frequency, i.e., the Overhauser field, at NMR conditions is measured as a function of the rf field amplitude.

In Fig. 4, the change of ω_L is plotted versus the square of the rf field. One should keep in mind that the nuclear spin polarization rate is only determined by the hyperfine interaction, while the spin depolarization rate strongly depends on the rf excitation power. For the ^{75}As resonance, the amplitude of nuclear spin depolarization is found to be constant over the whole rf power regime measured. This is due to the fact that independent of the rf power, the relation $\tau_{\rm dep} \ll \tau_{\rm pol}$ holds [1]. In contrast, in the case of the nonfundamental resonances, the change of the nuclear field strongly depends on the rf power. The nuclear spin depolarization is suppressed if the rf field amplitude is on the

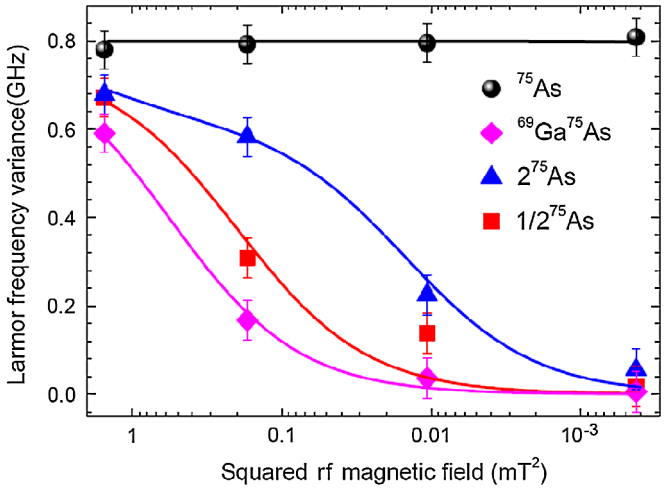

FIG. 4 (color online). Larmor frequency variation under NMR conditions versus the squared rf magnetic field. Lines are a guide to the eyes.

order of 0.01 mT or below. In this regime, τ_{dep} becomes much larger than τ_{pol} and ΔB_N becomes negligible.

This work has been financially supported by the German research foundation (DFG) within the priority program No. SPP1285 "Semiconductor Spintronics" and No. SFB491.

*Corresponding author.
yuansen.chen@uni-due.de

[1] A. Abragam, *The Principles of Nuclear Magnetism* (Oxford University Press, Oxford, 1961).
[2] M. A. Nielson and I. L. Chuang, *Quantum Computation and Quantum Information* (Cambridge University Press, Cambridge, 2002).
[3] D. D. Awschalom, D. Loss, and N. Samarth, *Semiconductor Spintronics and Quantum Computation* (Springer-Verlag, Berlin, 2002).
[4] O. Krebs, P. Maletinsky, T. Amand, B. Urbaszek, A. Lemaître, P. Voisin, X. Marie, and A. Imamoglu, Phys. Rev. Lett. **104**, 056603 (2010).
[5] R. I. Dzhioev and V. L. Korenev, Phys. Rev. Lett. **99**, 037401 (2007).
[6] P. Maletinsky, M. Kroner, and A. Imamoglu, Nature Phys. **5**, 407 (2009).
[7] M. N. Makhonin, E. A. Chekhovich, P. Senellart, A. Lemaitre, M. S. Skolnick, and A. I. Tartakovskii, Phys. Rev. B **82**, 161309(R) (2010).
[8] F. Meier and B. P. Zakharchenya, *Optical Orientation* (North-Holland, New York, 1984).
[9] S. E. Hayes, S. Mui, and K. Ramaswamy, in Special issue on New Developments in Magnetic Resonance, edited by S. Kuehn, S. A. Hickman, and J. A. Marohn [J. Chem. Phys. **128**, 052203 (2008)].
[10] V. K. Kalevich, V. D. Kul'kov, I. A. Merkulov, and V. G. Fleisher, Sov. Phys. Solid State **24**, 1195 (1982).
[11] H. Sanada, Y. Kondo, S. Matsuzaka, K. Morita, C. Y. Hu, Y. Ohno, and H. Ohno, Phys. Rev. Lett. **96**, 067602 (2006).
[12] V. L. Berkovits and V. I. Safarov, JETP Lett. **26**, 256 (1977).
[13] S. K. Buratto, J. Y. Hwang, N. D. Kurur, D. N. Shykind, and D. P. Weitekamp, Bull. Magn. Reson. **15**, 190 (1993).
[14] M. Eickhoff, B. Lenzmann, D. Suter, S. E. Hayes, and A. D. Wieck, Phys. Rev. B **67**, 085308 (2003).
[15] Y. S. Chen, S. Halm, E. Neshataeva, T. Kümmell, G. Bacher, M. Wiater, T. Wojtowicz, and G. Karczewski, Appl. Phys. Lett. **93**, 141902 (2008).
[16] Y. S. Chen, J. Huang, D. Reuter, A. Ludwig, A. D. Wieck, and G. Bacher, Appl. Phys. Lett. **98**, 081911 (2011).
[17] D. Paget, G. Lampel, and B. Sapoval, Phys. Rev. B **15**, 5780 (1977).
[18] As the change of the Larmor frequency due to nuclear spin depolarization at resonance is comparable for σ^+ and σ^- excitation (see, e.g., data for ^{75}As), we conclude that for linear polarized excitation the deviation between the optically injected electron spin polarization and the equilibrium electron spin polarization and thus the nuclear spin polarization is rather small compared to the case of circular-polarized pumping.
[19] J. Strand, X. Lou, C. Adelmann, B. D. Schultz, A. F. Isakovic, C. J. Palmstrm, and P. A. Crowell, Phys. Rev. B **72**, 155308 (2005).
[20] P. T. Eles and C. A. Michal, Prog. Nucl. Magn. Reson. Spectrosc. **56**, 232 (2010).
[21] J. H. Shirley, Phys. Rev. **138**, B979 (1965).
[22] D. Paget, T. Amand, and J.-P. Korb, Phys. Rev. B **77**, 245201 (2008).
[23] Y. S. Chen, M. Wiater, G. Karczewski, T. Wojtocicz, and G. Bacher, Phys. Status Solidi B **247**, 1505 (2010).
[24] J. Lu, M. J. R. Hoch, P. L. Kuhns, W. G. Moulton, Z. Gan, and A. P. Reyes, Phys. Rev. B **74**, 125208 (2006).
[25] V. K. Kalevich, K. V. Kavokin, and I. A. Merkulov, in *Spin Physics in Semiconductors*, edited by M. l. Dyakonov (Springer, Heidelberg, 2008).
[26] H.-P. Breuer and F. Petruccione, *The Theory of Open Quantum Systems* (Oxford University Press, New York, 2007).
[27] R. K. Wangsness, Phys. Rev. **104**, 857 (1956).
[28] D. Paget, Phys. Rev. B **25**, 4444 (1982).